IJCRT.ORG ISSN : 2320-2882

INTERNATIONAL JOURNAL OF CREATIVE RESEARCH THOUGHTS (IJCRT)

An International Open Access, Peer-reviewed, Refereed Journal

INVESTIGATION OF ECCENTRICALLY LOADED CFS SIGMA BEAMS

[1] Mohamed Ismail, [2] Ali Hammad, [3] S. M. Ibrahim

[1] Research Assistant, [2] Assistant Professor, [3] Professor

Department of Structural Engineering,

[1] Ain Shams University, Cairo, Egypt

Abstract: Cold-Formed Steel (CFS) has become increasingly popular in the construction industry due to its sustainable and cost-effective characteristics, serving as a viable alternative to traditional building materials. Optimizing the profile of CFS sections has proven effective in enhancing the structural efficiency of members by mitigating buckling instabilities that could lead to premature failure. A great example of such optimization is found in the CFS sigma section, which differs from the conventional lipped C-section by incorporating a web-stiffening feature to enhance resistance to both local and distortional buckling. This experimental investigation delves into the behavior of CFS sigma beams under eccentric loading, a condition that induces combined bending and torsional moments. The research seeks to interpret prevalent failure modes in these beams and assess the impact of modifying geometric parameters on their load-bearing capacity. A carefully designed test setup was employed to ensure compliance with prescribed loading and boundary conditions. Concurrently, numerical models were developed using Abaqus Finite Element Analysis (FEA) software to simulate the behavior of the tested beams. These models were calibrated against the experimental results, enabling the generation of load-displacement curves to offer deeper insights into the research findings.

Index Terms - Cold-Formed Steel Sections, Sigma Section, Local Buckling, Distortional Buckling, ABAQUS, Finite element analysis, Eccentric beam loading.

I. INTRODUCTION

The utilization of Cold-Formed Steel (CFS) in structural applications has been expanding notably in recent years, presenting a compelling alternative to the traditional use of heavier hot-rolled steel members. Forged from sheets or rolls through press braking or roll forming techniques, studies have diligently sought to optimize the profiles of CFS sections. The primary objective is to maximize their usability and augment their strength in response to applied loads by mitigating local buckling instabilities, thereby enhancing their strength-to-weight ratio.

CFS open sections typically exhibit a single axis of symmetry, leading to a divergence between the locations of the shear center and the center of gravity. Under load, CFS beams are prone to torsional moments, supplementing the conventional bending moment action, as the applied loads typically act at a distance from the shear center.

In previous research, Put et al. [1] conducted experiments on various cold-formed steel channel beams, including eccentrically loaded midspan, unbraced, simply supported, and concentrically loaded configurations. A specialized loading apparatus applied transverse loads precisely at the shear center and allowing for both positive and negative eccentricities. They found a correlation between the failure modes observed in the tested beams and the direction of load eccentricity. Specifically, negative eccentricity (away from the web) is associated with the failure of local buckling in the compression lip. This occurs because the shear center axis moves away from the initial web plane, leading to increased compression in the top flange lip. On the other hand, positive eccentricity (toward the web) is linked to the failure of local buckling at the compression flange-web junction. In this case, the shear center axis moves toward the initial web plane, causing increased compression in the top flange-web junction. Additionally, Finite Element Analysis was

employed to develop an interaction equation for approximating the strength limits of the investigated sections. Q. Liu [2] conducted a series of experimental tests on the CFS sigma profile when employed as purlins. The investigation encompassed an exploration of the structural behavior of these profiles as continuous beams, their flexural characteristics when affixed to corrugated roof sheets, as well as an analysis of sleeve connections. Key parameters such as moment capacity and rotational behavior were investigated to provide a comprehensive understanding of the performance of CFS sigma profiles in practical applications. Subsequently, Wan and Mahendran [3] embarked on a thorough examination involving nine laboratory tests on light steel beams (LSB) subjected to combined bending moment and torsion, as depicted in Figure *1*. Their experimental setup featured concentrated vertical load applied at the mid-span of the beam, eccentric from the shear center. A specialized test rig was employed to control the value of the load eccentricity. To complement the experimental work, the tested beams were modeled using Finite Element Method (FEM) software, employing an equivalent loading method involving a transverse load and a horizontal couple to simulate the eccentric load conditions. Building upon this foundation,

Wan et al. (2015) [4] extended their inquiry to encompass a total of 24 simple beams. Twelve tests each were conducted on conventional C-lipped CFS beams and Z-lipped CFS beams under the combined influence of bending moment and torsion. Employing a loading methodology similar to that used in testing LSB beams, three different eccentricities were considered for each beam configuration, across two distinct spans.

Moreover, several design standards offer practical guidelines for considering the impact of torsional stresses on structural members, although these methods often involve indirect approaches, The AISI S100 [5] provides comprehensive guidance on how to calculate and apply a torsional reduction factor, "R" for the members' flexural strength, expressed as,

$$R = \frac{f_{\text{bending,max}}}{f_{bending} + f_{torsion}} \leq 1 \quad (1)$$

where, "$f_{bending,max}$" represents the greatest bending stress observed at the outermost part of the member. "$f_{bending}$" indicates the bending stress at a specific point inside the cross-section where the combined influence of bending and torsion results in the highest stress. Lastly, "$f_{torsion}$" characterizes the stress due to torsional warping at the same location in the cross-section, where the combined effects of bending and torsion produce the most significant stress levels. GB 50018-2002 [6], offers an alternative approach for the analysis of flexural members in situations where the load-bearing direction deviates from the bending center while remaining parallel to the main axis. In this context, the following formulas are employed in section 5.3.2 to assess the normalized ratios for the strength and stability of such members:

$$\frac{M}{M_b} + \frac{B}{B_y} \leq 1 \quad (2)$$

In these formulas, M represents the bending moment at the specified section, B is the bi-moment, M_b represents the bending capacity of the member, and B_y stands for the bi-moment capacity of the member. The Eurocode 3 developed by the European Committee for Standardization, Part 1-3 provides essential provisions concerning the upper limits governing the complex impacts of longitudinal and shear stresses within structural members subjected to both bending and torsion. These regulations are encapsulated in the following interaction equation:

$$\sqrt{{\sigma_{tot,Ed}}^2 + 3{\tau_{tot,Ed}}^2} \leq 1.1 * \frac{f_{ya}}{\gamma_{MO}} \quad (3)$$

In this equation, $\sigma_{tot,Ed}$ signifies the design total direct stress, calculated based on the relevant effective cross-section, $\tau_{tot,Ed}$ denotes the design total shear stress, established with respect to the gross cross-section. Moreover, f_{ya} represents the average yield strength of the material, and γ_{MO} serves as the material safety factor.

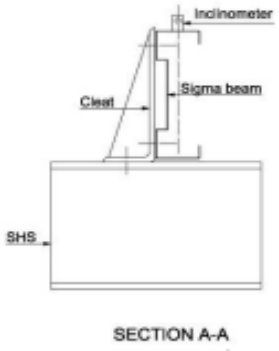

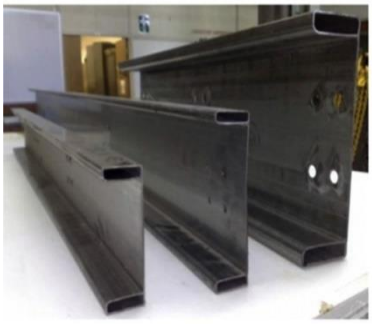

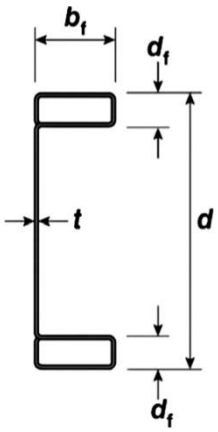

(b) LSB beams tested in **[3]**

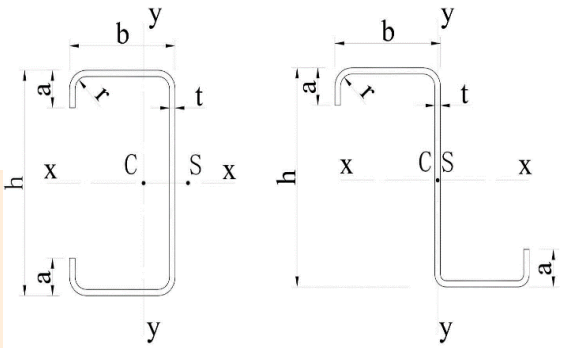

Figure 1: Previous research

II.EXPERIMENTAL TESTS

2.1 Set-up and Loading

2.1.1 Tested Profiles

This study aims to investigate experimentally the behavior of simply supported CFS beams featuring a sigma profile as the beam section, as depicted in Figure 2. These beams are subjected to an eccentric load at the mid-span denoted as “P”, positioned 50 mm away from the cross-section’s shear center outside the beam. Table 1 outlines the dimensions of the tested specimens in this research. The initial specimen had a total height of 200 mm and a flange width of 60 mm, with a stiffening distance to beam flange width ratio (a/B) of 0.25. Specimen 2 is designed to investigate the impact of increasing the stiffening distance on the beam's capacity, achieved by elevating the a/B ratio to 0.5, placing the shear center in proximity to the cross-section's web location. Specimens 3 and 4 are modifications of specimens 1 and 2, respectively, maintaining identical dimensions except for an increase in beam height to 220 mm by increasing the top and bottom portions of the web only. All four profiles were tested for two different thicknesses: 1.8 mm and 2.5 mm, respectively.

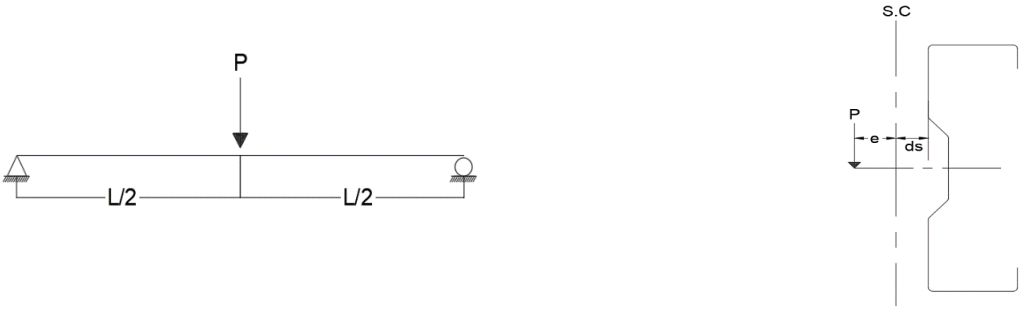

Figure 2: Eccentric Loading

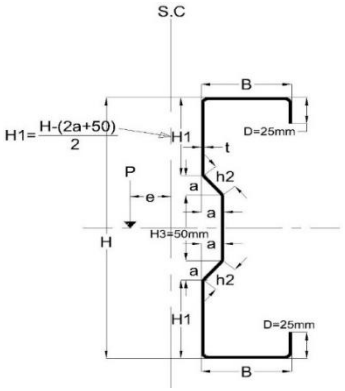

Figure 3: Tested Sigma profile

Table 1: Tested Specimens

Specimen no.	L (mm)	T (mm)	H (mm)	B (mm)	D (mm)	H1 (mm)	H2 (mm)	H3 (mm)	a (mm)	a/B
1	1200	1.8 & 2.5	200	60	25	60	20.2	50	15	0.25
2						45	41.4		30	0.5
3			220			70	20.2		15	0.25
4						55	41.4		30	0.5

2.1.2 Test Set-up

The experimental setup shown in Figure 4 was thoroughly designed to achieve the desired combined bending and torsion action. A loading system was accurately constructed to induce eccentric loading. The loading apparatus comprises a vertical arm composed of sturdy plates and reinforcing stiffeners. This vertical arm is affixed to a horizontal arm through a pin connection, enabling unrestricted rotation of the horizontal arm while the vertical load maintains a gravitational direction during the entirety of the test. The horizontal arm is constructed from two perpendicular welded plates, with one connected to the vertical arm through a pin connection, and the other securely fastened to the beam's web using bolts, acting as a head plate. The length of the horizontal arm controls the value of the loading eccentricity. The maximum bending moment value was calculated to be at the loading location and equaled PL/4, with L consistently representing the clear span of the beam, maintained at 1200 mm, while the torsional moment value was determined to be equal to P*e, with “e” representing the eccentricity of the load measured from the shear center of the cross-section.

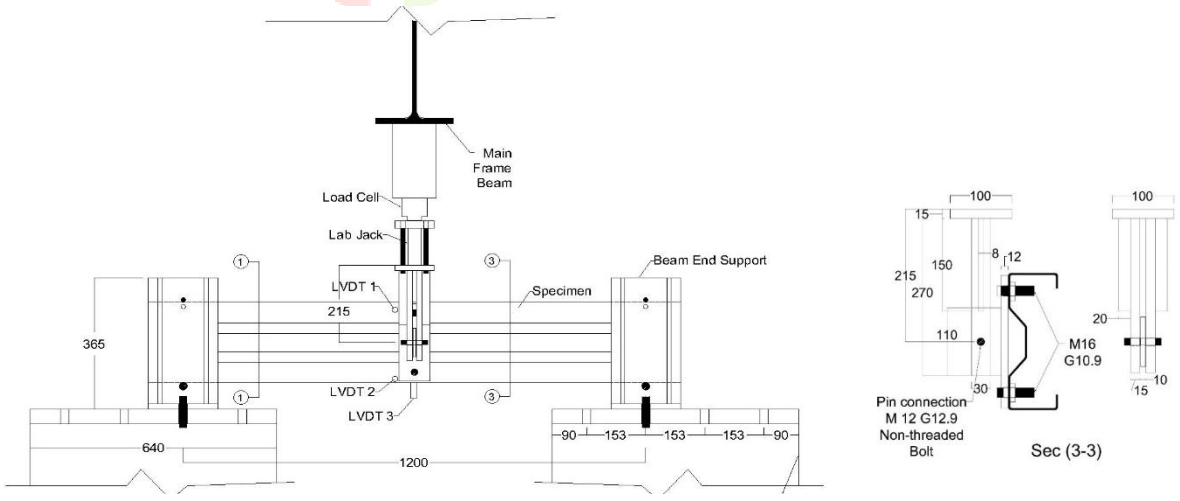

(a) Typical Test Set-up

(b) Front view of the tested beams

(c) Test rig and transducers

Figure 4: Test Set-up

To track the occurring deformations during experimental testing, a system of three Linear Variable Differential Transformers (LVDTs) was employed as shown in Figure 4. Positioned with precision, the first LVDT, oriented horizontally near the web-to-top flange junction, accurately measured lateral displacements along the top flange, providing crucial data on its deformation. Similarly, the second LVDT, located near the web-to-bottom flange junction, captured lateral displacement of the bottom flange. The third LVDT, positioned vertically and perpendicular to the bottom flange, observed beam deflection during experiments, offering valuable insights into performance under applied loads. This combination of LVDTs and the robust apparatus design guaranteed precise and reliable execution of experiments. Finally, a load cell was attached to the loading jack to record the applied load's value.

2.1.3 Supports

The test supports shown in Figure *5* were designed to replicate the end conditions of a simple beam. In this configuration, the lower flange of the sigma beam is precisely positioned on a lower roller, a stainless rod with a 20 mm diameter. Simultaneously, the upper part of the beam is securely anchored in place by an upper roller. Functioning as pivotal components, these rollers allow the beam to bend and warp in the longitudinal direction.

To maintain requisite restraints and ensure the reliability of the testing conditions, the two sides of the cross-section are effectively confined by two side plates, each with a thickness of 10 mm and a width of 180 mm. These side plates are additionally reinforced with 8 mm vertical stiffeners, augmenting their rigidity and the overall stability of the arrangement.

The combination of side plates and vertical stiffeners restrict rotations about the longitudinal axis of the beam. Moreover, these elements prevent displacements in both the vertical and lateral planes. The side plates and stiffeners were welded to 15 mm base plates. The entire assembly of supporting elements is then securely affixed to the test support table using high-strength bolts, ensuring the stability and consistency of the setup throughout the experiments.

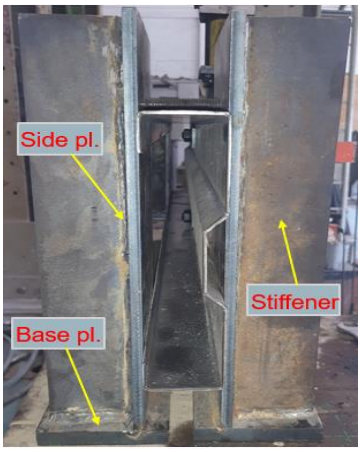

(a) Side View

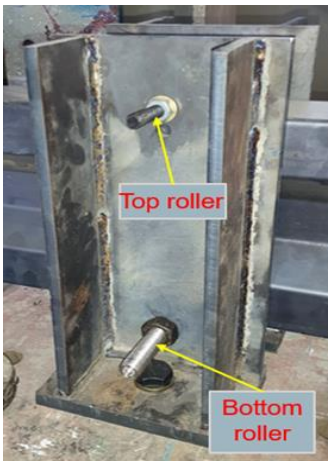

(b) Elevation

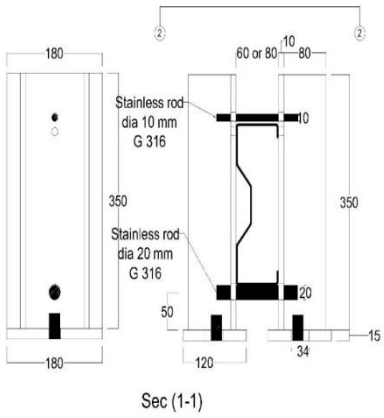

(c) Dimensions

Figure 5: Test Supports

2.1.4 Testing and Results

In the typical test procedure, the beam was carefully positioned within the supporting system, ensuring precise alignment and stability. The supporting plates were adjusted to securely enclose the beam ends according to design specifications. Connection to the loading rig and clamping plates at mid-span was achieved through bolts, with thorough inspections to confirm their presence and proper tightening. Employing a spirit level and angle gauge ensured accurate positioning of all elements. The LVDTs were positioned as specified, and the transverse vertical load was systematically applied using a hydraulic jack. Throughout loading, readings from the LVDTs and load cell were continuously recorded, even after reaching peak load, to capture post-peak plastic behavior. The resulting load versus lateral displacements of the flanges was plotted. The beams exhibited concurrent mid-span twisting and deflection under increasing loads, followed by a decline after reaching peak capacity. Remarkably, lateral displacement of the top flange consistently exceeded that of the bottom flange at peak load. The typical failure mode involved cross-sectional twisting governed by warping torsion, often accompanied by local buckling in the top flange under compression, occasionally extending to the top lip. Ultimate test loads are summarized in Table *3*. Figure 6 shows the peak loads vs lateral flange displacements for the tested specimens, while Figure 7 illustrates the common failure mode observed in the tested beams.

The results indicate that increasing the ratio of a/B to 0.5, thereby bringing the cross-section's shear center closer to the web extension, significantly enhanced the capacity of the tested beams. Likewise, augmenting the beam thickness demonstrated a clear enhancement in capacity, while the increase in beam height resulted in a slight change in the beams' capacity.

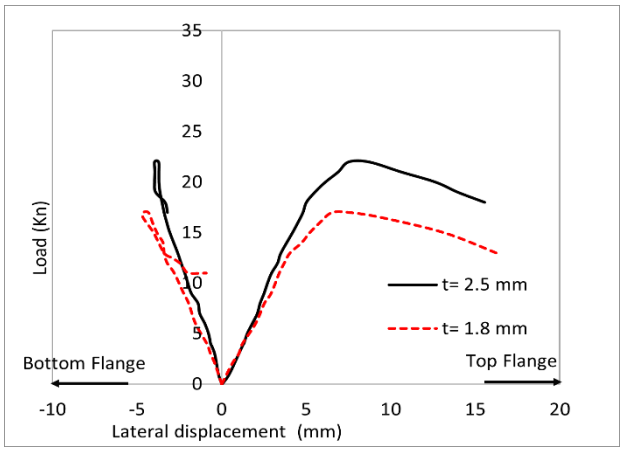

(a) Specimen 1

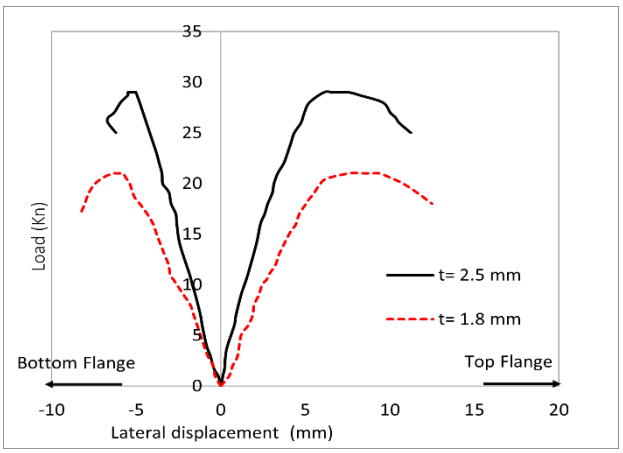

(b) Specimen 2

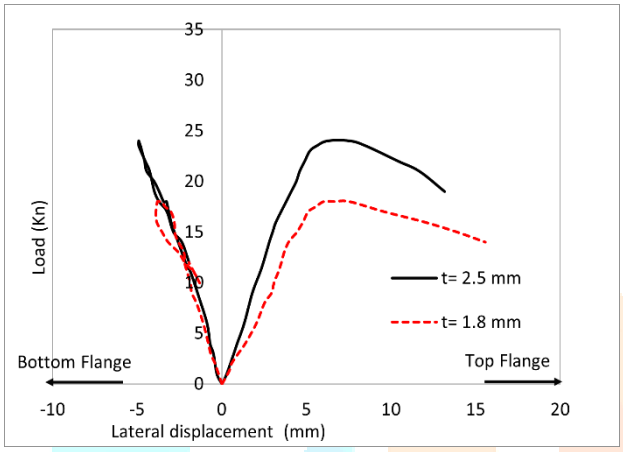

(c) Specimen 3

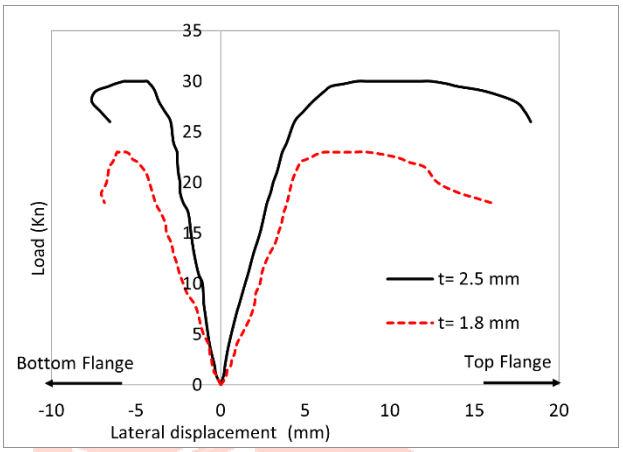

(d) Specimen 4

Figure 6: Load vs Lateral displacement for the tested beams

Figure 7: Typical Failure mode of the tested beams

III. VERIFICATION

3.1 FEM modeling build-up

Constructing finite element models to replicate the test configuration and procedures, followed by the validation of the obtained results against the real tests, forms a strong methodology to broaden the implications of the experimental program. Abaqus CAE software was employed to construct finite element models for the beams under examination.

To define the beam profiles, a 4-node shell element S4R with five degrees of freedom from the Abaqus library, featuring reduced integration, was utilized. This specific element is well-suited for analyzing thin-

walled members. The cross-sectional mesh consisted of a rectangular grid with a width of 5 mm and a length of 10 mm for the flat portions, while a denser mesh was employed for the curved fillets. The dimensions of the modeled cross-sections were based on centerline measurements, ensuring an accurate representation of the beam profiles.

To replicate the applied loads in the test, an eccentric load was replaced by a transverse shear load and a moment. The moment's magnitude equaled the product of the eccentric load and the distance from the shear center. This induced moment was modeled using two opposing horizontal forces applied at the junctions of the web to the beam's top and bottom flanges. The forces were adjusted to be equivalent to the moment value divided by the cross-section's height.

The loading method adopted in the finite element models is depicted in Figure 8. The experimental Boundary conditions were simulated by restraining nodes at the beam ends in contact with the test supporting elements. Specifically, the top and bottom portions of the web, as well as the top and bottom flanges and lips, were prevented from displacements in the transverse XY-plane and rotations about the longitudinal Z-plane. Additionally, nodes on the top and bottom portions of the web at the mid-section were restricted from translation in the longitudinal Z-direction.

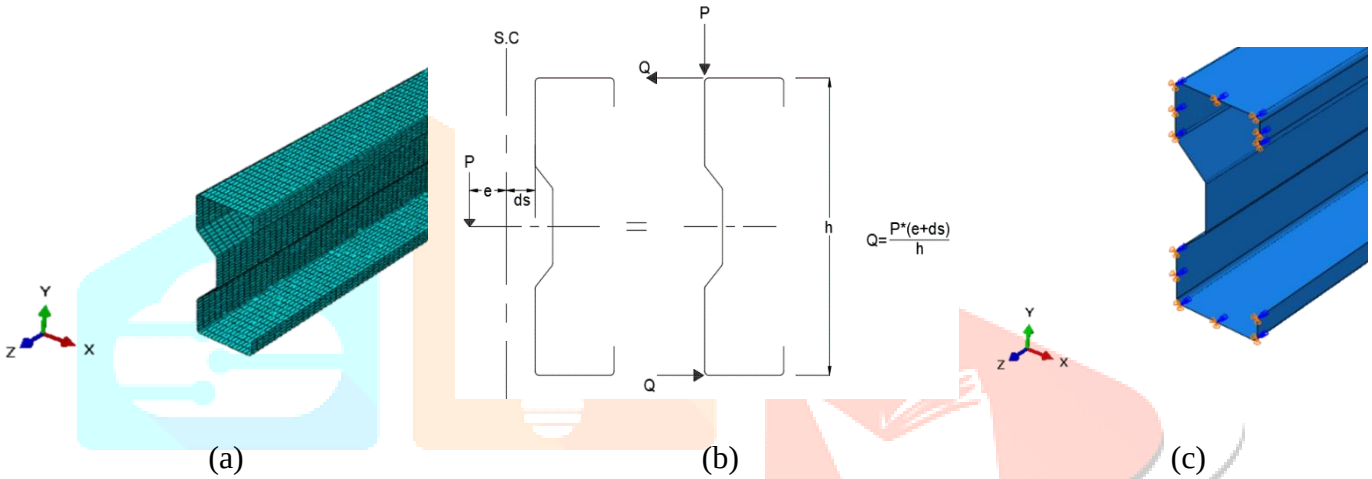

(a) (b) (c)

Figure 8: (a) Meshing, (b) Equivalent Loading & (c) End nodes conditions.

3.2 Material properties

A bi-linear stress-strain model was employed to define the material properties of the beams under examination. To establish this model, tensile coupon tests were initially conducted on samples extracted from the sheets utilized in manufacturing the sigma beams. These samples underwent tension loading until fracture. Table *2* documents the average yield and ultimate strength of the tested coupons, along with the percentage of elongation.

The average yield strength obtained from these tests was utilized to define the material yield strength in the finite element models. Additionally, the average Young's modulus was determined to be 206,000 MPa. The post-yield line was assumed to have a slope of zero, implying the adoption of an elastic-perfectly plastic material model as shown in Figure 9.

Table 2: Tensile Coupon results

Fy (Mpa)	Fu (Mpa)	δ %
339.11	433.05	33.72

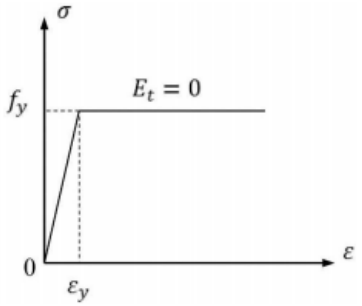

Figure 9: Bi-linear Stress-strain curve

3.3 Analysis and results

The inclusion of initial imperfections is crucial in anticipating the behavior of thin-walled elements undergoing nonlinear analysis. To address this, a linear buckling analysis was initially conducted on the modeled beams using Abaqus' linear perturbation buckle procedure to obtain key buckling modes and eigenvalues. The critical buckling mode was then employed to introduce initial imperfections during the subsequent nonlinear analysis, with an amplification factor of -L/1000, which is particularly suitable for capturing the twisting behavior exhibited by the tested beams.

For the nonlinear analysis of the modeled beams, the Static-Riks Abaqus procedure was employed, incorporating large displacements and arc length control. Table *3* provides a comparison between the ultimate loads of the tested specimens and those obtained from the Finite Element Models (FEM).

Figures 10-13 depict the load versus lateral displacement curves for the tests, contrasting them with the results from the FEM. The findings indicate that the FEM models effectively predicted the beams' capacity and lateral deformations, underscoring the reliability of the simulation in capturing the structural behavior.

Table 3: Ultimate loads

Specimen no.	t (mm)	P_{EXP} (KN)	P_{FEM} (KN)	P_{EXP}/ P_{FEM}
1	1.8	17	16.69	1.019
	2.5	22	21.05	1.045
2	1.8	21	19.03	1.104
	2.5	29	29.90	0.970
3	1.8	18	18.44	0.976
	2.5	24	22.82	1.052
4	1.8	23	22.03	1.044
	2.5	30	29.28	1.025
Mean				1.029
Deviation				0.040

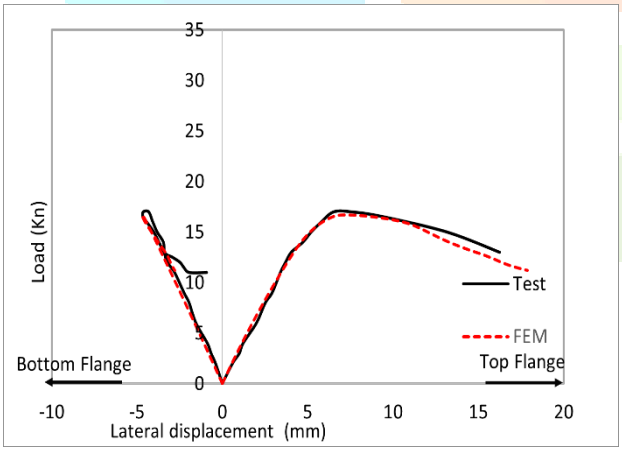

(a) t = 1.8 mm

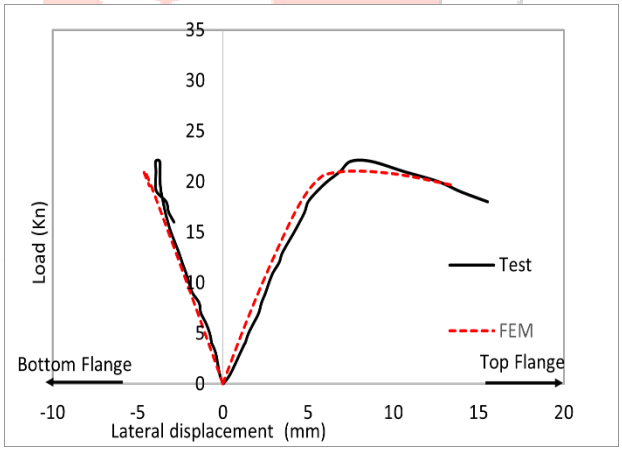

(b) t = 2.5 mm

Figure 10: Specimen 1 Test vs FEM.

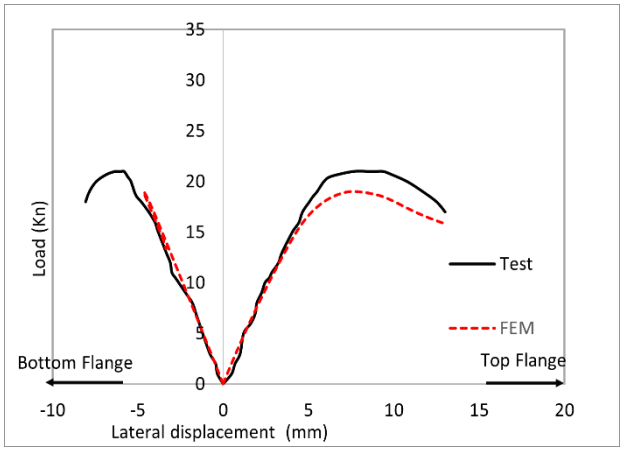

(a) t = 1.8 mm

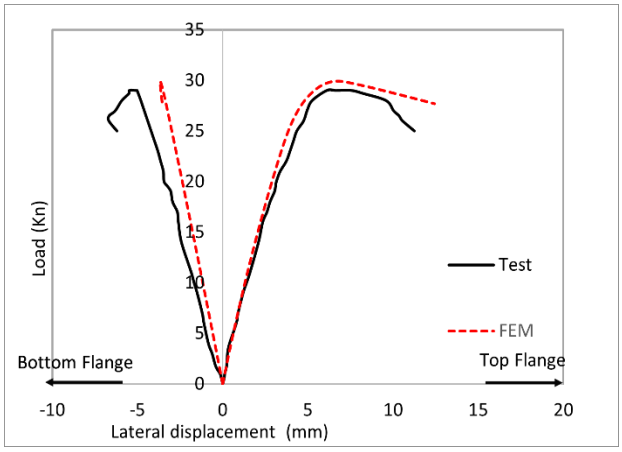

(b) t = 2.5 mm

Figure 11: Specimen 2 Test vs FEM.

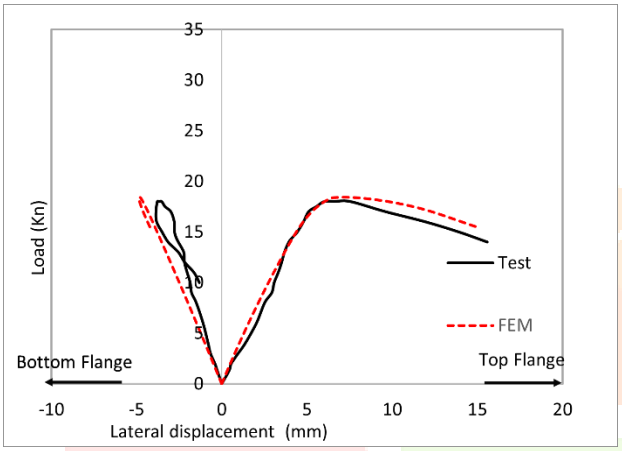

(a) t = 1.8 mm

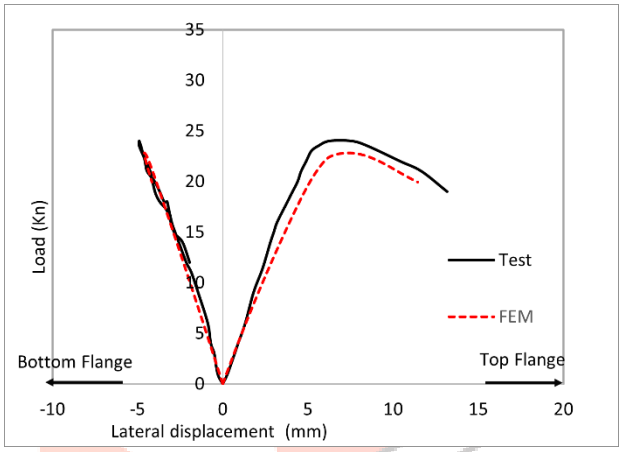

(b) t = 2.5 mm

Figure 12: Specimen 3 Test vs FEM.

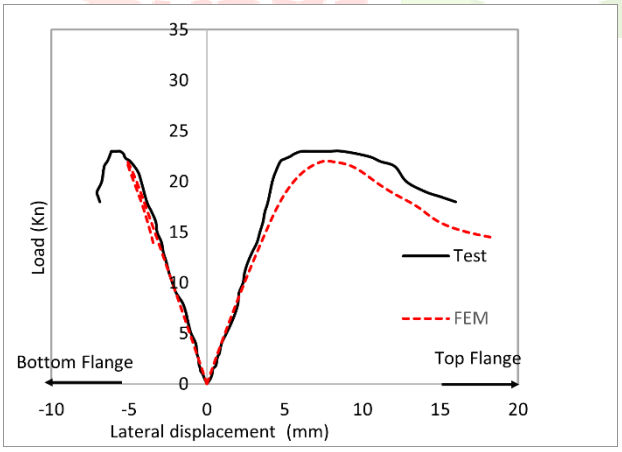

(a) t = 1.8 mm

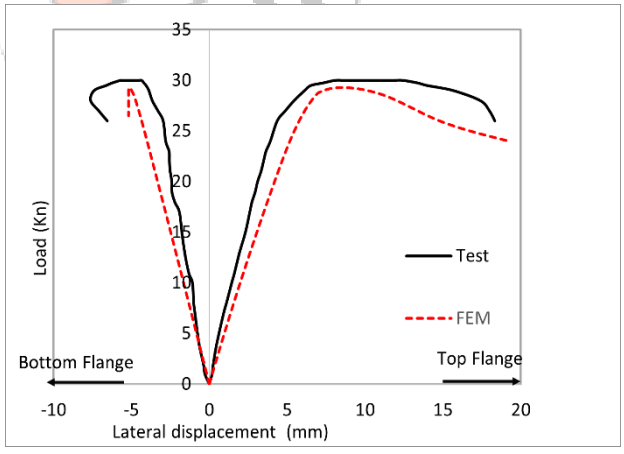

(b) t = 2.5 mm

Figure 13: Specimen 4 Test vs FEM.

IV. CONCLUSION

This paper provides a thorough examination of the behavior of cold-formed steel sigma beams under eccentric transverse loading, a scenario involving complex interactions of bending and torsional moments. The experimental program investigated 4 sigma specimens subjected to mid-span eccentric loading, where the 4 profiles were tested at thicknesses of 1.8 and 2.5 mm and variable cross-sectional parameters. The eccentric load, positioned 50 mm from the cross-section's shear center, was gradually applied to capture post-

peak behavior. The predominant failure mode involved cross-sectional twisting, primarily driven by warping torsion, often accompanied by local buckling in the top flange under compression and potentially in the top lip. Results indicate that increasing the a/B ratio to 0.5 significantly enhanced beam capacity by bringing the shear center closer to the web extension. Similarly, increasing beam thickness notably improved capacity, while an increase in beam height had a marginal impact. Moreover, simplified non-linear Finite Element Models were created for the tested beams, using Abaqus FEA software adopting an equivalent loading method, closely matched peak loads and lateral displacements with the tested specimens.

REFERENCES

[1] B.M. Put, Y.L. Pi, N.S. Trahair, Bending and torsion of cold-formed channel beams, J. Struct. Eng. 125 (1999) 540-546.

[2] QIANG LIU, "Structural Analysis and Design of Cold Formed Steel Sigma Purlins," Thesis, no. September 2012

[3] Hong-Xia Wan a, Mahen Mahendran**, "**Behaviour and strength of hollow flange channel sections under torsion and bending,". In: Thin-Walled Structures 94, vol. 94, p. 612-623, 2015.

[4] Wan, Hong Xia, Bin Huang, and Mahen Mahendran (2021). "Experiments and numerical modelling of cold-formed steel beams under bending and torsion". In: Thin-Walled Structures vol.161, p. 107424, 2021.

[5] American Iron and Steel Institute (2020). S100-16 (R2020): North American Specification for the Design of Cold-formed Steel Structural Members. Washington, DC, U.S.A.

[6] Ministry of Construction of the P.R.C and General Administration of Quality Supervision, In section and Quarantine of the P.R.C (2002). Technical code of cold-formed thin-wall steel structures. Beijing, China, pp. 1–93.

[7] American Society for Testing and Materials. (2016). Standard test methods for tension testing of metallic materials. E8/E8M.West Conshohocken.

[8] ABAQUS, 2014. ABAQUS User's Manual V. 6.14.

[9] B.W. Schafer, Z. Li, C.D. Moen. "Computational modeling of cold-formed steel", In: Thin-Walled Structures vol.48, p. 752-762, 2010.

[10] Zienkiewicz, O.C., Taylor, R.L., and Zhu, J.Z. (2005). The finite element method: Its basis and fundamentals. Butterworth-Heinemann.

[11] Bathe, K.J. (1996). Finite element procedures. Prentice-Hall, Inc.

[12] Riks, E. (1979). An incremental approach to the solution of snapping and buckling problems. International Journal of Solids and Structures, 15(7-8), 529-551.